Acta Crystallographica Section D
Biological Crystallography
ISSN 0907-4449

Resolution improvement of X-ray diffraction data of crystals of a vesicular stomatitis virus nucleocapsid protein oligomer complexed with RNA

Todd J. Green and Ming Luo*

Department of Microbiology, School of Medicine, University of Alabama at Birmingham, 1025 18th Street South, Birmingham, AL 35294, USA

Correspondence e-mail: mingluo@uab.edu

Received 21 December 2005
Accepted 23 February 2006

Vesicular stomatitis virus (VSV) is a non-segmented negative-stranded RNA virus. The nucleocapsid (N) protein of VSV is found tightly associated with the viral genomic RNA and this complex serves as the template for transcription and replication. A method for the soluble expression of the N protein in *Escherichia coli* has previously been reported. An N protein–RNA oligomer was isolated from this system, the stoichiometry of which was determined to be ten molecules of the N protein bound to approximately 90 nucleotides of RNA. Here, the crystallization of this protein–nucleic acid complex is presented. The crystals belong to space group $P2_12_12$, with unit-cell parameters a = 165.65, b = 235.35, c = 75.71 Å and a diffraction limit of 6 Å. Self-rotation function analysis has shown the oligomer to have tenfold rotational symmetry. In a search to identify heavy-atom derivatives, uranyl acetate was discovered to stabilize the crystals, giving them an increase in diffraction limits to beyond 2.9 Å. Based on the internal symmetry of the oligomer, the size of the oligomer determined previously by negative-stained electron microscopy, the space-group symmetry and packing considerations, the packing arrangement in the crystal has been determined.

1. Introduction

VSV is a non-segmented negative-stranded RNA virus belonging to the rhabdovirus family. The 11 161 nucleotide genome of VSV (Huang & Wagner, 1966) contains five genes and is encapsidated by the N protein to form the ribonucleoprotein (RNP) complex. The entire RNP of VSV contains 1258 molecules of the N protein, each of which is bound to nine bases of RNA (Thomas *et al.*, 1985). RNAse protection assays and chemical probing studies have indicated that the N protein binds to the ribose-phosphate backbone of the RNA (Green *et al.*, 2000; Iseni *et al.*, 1998; Keene *et al.*, 1981). This binding arrangement results in the protection of the ribose-phosphate backbone, while allowing the bases of the nucleotides to be exposed and available to the viral polymerase during transcription and replication. This is essential as the RNP, not the naked viral genomic RNA, is the template for the viral polymerase, a complex between the large polymerase subunit (L) and the viral phosphoprotein (P) (Emerson & Wagner, 1972; Emerson & Yu, 1975) and other factors. Transcription is carried out by a complex between L, P and host factors which include heat-shock protein 60, elongation factor 1α and mRNA-capping guanylyltransferase (Qanungo *et al.*, 2004). Collectively, these components make up the transcriptase. The replicase is composed of a tripartite complex between the N, P and L proteins (Qanungo *et al.*,

2004). Both of these processes use the RNP as the active template.

In addition to being involved in the processes of transcription and replication, the N protein is also a structural component of the virus. The N proteins from VSV and rabies virus, another rhabdovirus, have been studied extensively in order to discover some of the structural details of nucleocapsid proteins from negative-stranded viruses. Blumberg and Kolakofsky developed a method to refold VSV N protein in the presence of high-molar salt and viral leader RNA (Blumberg & Kolakofsky, 1983). In a separate set of experiments, our group has expressed the N protein along with the P protein in *Escherichia coli* (Green *et al.*, 2000). Electron photomicrographs showed that the material in each of these cases was oligomeric and had a toroidal morphology. Similarly, Iseni and coworkers overexpressed the rabies virus N protein in the baculovirus system (Iseni *et al.*, 1998). N-protein oligomers were isolated from this system and like the N protein of VSV predominantly contained ten monomers of the N protein. These experiments were followed up with further structural studies using the techniques of cryo-electron microscopy (EM) and three-dimensional image reconstruction (Schoehn *et al.*, 2001). Recently, our group has published the structure of a VSV N protein–RNA oligomer determined by negative-stain image-reconstruction techniques (Chen *et al.*, 2004). The structure of VSV N, like the rabies N protein, showed that the N protein has a bilobed shape with two contact sites for each neighboring N protein and the protein disc had a tenfold rotational symmetry. These observations are consistent with scanning transmission EM analysis of nucleocapsids isolated from virions (Thomas *et al.*, 1985). The N protein was shown to have a wedge-shaped bilobed structure that was elongated along one direction. To date, high-resolution details of the N protein have not been available.

In a previous report, we showed that the N protein can be produced under conditions in which the majority of the protein is in a soluble encapsidation-competent form in *E. coli* if it is expressed concomitantly with the P protein (Green *et al.*, 2000). A soluble complex between the N and P proteins and a short cellular RNA was isolated and characterized. The P protein could be dissociated from the N protein–RNA complex, resulting in the N protein–RNA complex remaining intact. The complex contained ten molecules of the N protein and an RNA of ∼90 nucleotides. This N protein–RNA complex has been the focus of structural studies. In this report, we summarize the crystallization and X-ray analysis of this protein–nucleic acid complex. In addition, we report a procedure for successful extension of the diffraction limits of the crystals.

2. Materials and methods

2.1. Preparation and purification of VSV N protein

The isolation and purification of VSV N protein–RNA complexes were carried out as described in Green *et al.* (2000). Briefly, VSV N protein was co-expressed with His-tagged VSV phosphoprotein (P) in *E. coli*. N/P protein–RNA complexes were purified by Ni-affinity chromatography. The protein–RNA complexes were then dialyzed in 0.1 *M* citrate buffer pH 4 containing 250 m*M* NaCl. This resulted in dissociation of the P protein from the N protein–RNA complex and precipitation of the P protein from the solution. Uncomplexed N protein–RNA complexes were dialyzed against 50 m*M* Tris buffer pH 7.5 containing 300 m*M* NaCl and isolated on a Sephacryl S-300 gel-filtration column. This purified sample was concentrated to 12 mg ml^{-1} for crystallization trials.

2.2. Crystallization and crystal preparation

Purified N protein–RNA complexes were screened for crystallization conditions using the hanging-drop vapor-diffusion method (McPherson, 1982) following the sparse-matrix grid screen (Jancarik & Kim, 1991) at 277 and 293 K. In each trial, 2 µl protein solution was mixed with 2 µl precipitating agent. Crystallization leads were optimized. Ultimately, the N protein–RNA complex was crystallized in 7–8%(*w*/*v*) polyethylene glycol (PEG) 3350 containing 250 m*M* sodium chloride buffered with 100 m*M* sodium acetate pH 4.5 at 293 K. Crystals grew in 2–7 d depending on the concentration of PEG 3350. Native crystals were cryoprotected stepwise in 10%(*w*/*v*) PEG 3350 containing 250 m*M* sodium chloride buffered with 100 m*M* sodium acetate pH 4.5 supplemented with glycerol at concentrations of 10, 12.5, 15 and 18%(*v*/*v*) followed by a short wash in 20%(*w*/*v*) PEG 3350 containing 250 m*M* sodium chloride buffered with 100 m*M* sodium acetate pH 4.5 supplemented with 20% glycerol. In order to approach phasing of the data, crystals were screened in mother liquor containing heavy atoms. In the presence of heavy atoms, crystals often cracked. Owing to the fragility of the crystals in the heavy-atom solutions, crystals were routinely soaked in low concentrations of heavy atoms initially and the concentrations increased over time. Specifically, native crystals were soaked stepwise in mother liquor containing 0.1, 0.3, 0.5, 1.0, 1.5 and 2.5 m*M* uranyl acetate at approximately 20 min intervals. Uranyl-containing crystals were cryoprotected in the same way as native crystals with the inclusion of 2.5 m*M* uranyl acetate in each cryosolution.

2.3. X-ray analysis

Native and uranyl-derivative diffraction data were collected on an R-AXIS IV image plate mounted on a Rigaku RU-200 rotating-anode generator (λ = 1.5418 Å) with a crystal-to-detector distance of 250 mm and an oscillation of 1°. Native diffraction data were also collected at the Advanced Photon Source (APS), BioCARS beamline 14-BM-C on a MAR 345 image plate with a crystal-to-detector distance of 440 mm and 1.5° oscillation (λ = 1.037 Å). Uranyl-derivative crystal data were also collected at APS, SERCAT beamline 22-ID (λ = 1.0 Å) on a MAR 300 CCD detector with a crystal-to-detector distance of 450 mm and 0.5° oscillation. The initial indexing and data-collection strategies were determined with *MOSFLM* (Leslie, 1992); subsequently, all raw frame data were processed with *DENZO* and *SCALEPACK* (Otwi-

nowski & Minor, 1997). Structure factors were calculated with *TRUNCATE* (French & Wilson, 1978). All data were collected at 100 K.

The self-rotation function was calculated with *GLRF* (Tong & Rossmann, 1997). To look for non-crystallographic twofold and tenfold symmetry, the κ angle was set at 180 and 36°, respectively, during the self-rotation function calculation. The Patterson integration radius was 40 Å and data in the resolution range 15.0–4.0 Å were used.

3. Results and discussion

The VSV N protein–RNA complex has previously been shown to have a disc-like morphology and was suggested to be composed of ten molecules of the N protein and a single strand of RNA of roughly 90 bases (Green *et al.*, 2000; Chen *et al.*, 2004). This complex was subjected to several screening procedures in order to identify crystallization conditions. The screens included home-designed sparse-matrix grid screens and the commercially available Hampton Crystal Screen kits I and II. Crystals were obtained in a variety of conditions from pH 4 to 9 in precipitants including PEG (of various molecular weights), 2-methyl-2,4-pentanediol (MPD) and ammonium sulfate. Interestingly, the complex could be crystallized in 8% PEG 3350, 250 m*M* sodium chloride in various buffers at pH values between 4 and 9. To generalize, conditions of lowered pH yielded single crystals with greater thickness, while crystals grown at pH 6 and above were always clusters of malformed needles. Variations of protein and precipitant concentration and the addition of additives such as glycerol, detergents and dioxane were all unsuccessful in slowing nucleation in the higher pH conditions. Since the crystallization of the needles could not be refined, these conditions were eventually abandoned.

Initial crystals obtained at low pH had poor diffraction profiles, with some having no detectable diffraction. Specifically, crystals grown in 0.1 *M* sodium acetate pH 4.6 with 0.02 *M* $CaCl_2$, 30%(*v*/*v*) MPD and crystals grown in 0.1 *M* citrate pH 5.6, 0.25 *M* NaCl, 22%(*v*/*v*) PEG 400 only diffracted to approximately 10 Å. Continued refinement of the crystallization conditions yielded large single crystals in 7–8%(*w*/*v*) PEG 3350 containing 250 m*M* sodium chloride buffered with 0.1 *M* sodium acetate pH 4.5. These crystals grew in 2–7 d depending on the concentration of PEG 3350 and the size of these crystals was as large as 1 mm in the long direction. An example of the N protein–RNA complex crystal from these conditions is shown in Fig. 1. These crystals routinely diffracted to at least 7.5 Å; however, upon screening of several hundred crystals an outlier was found to produce interpretable diffraction data to 6 Å. In the case of the native crystals, diffraction limits were similar regardless of the X-ray source (laboratory source or synchrotron). Oscillation diffraction images of native N protein–RNA complex crystals collected at our home source and at a synchrotron facility are shown in Figs. 2(*a*) and 2(*c*), respectively. Data were processed in space group *P*222. The exact choice of the space group was determined to be $P2_12_12$ based on systematic absences. The unit-cell parameters and data statistics for the highest resolution native data set are given in Table 1.

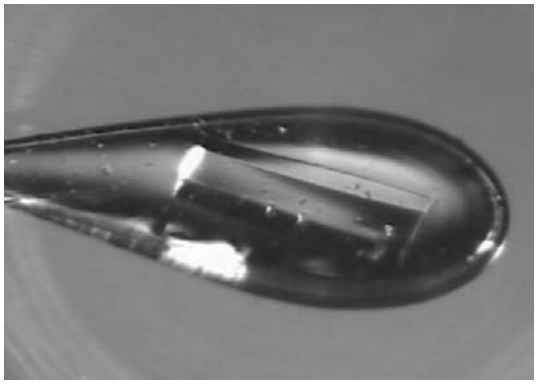

Figure 1
Crystal of the VSV N protein–RNA complex. The long dimension of the crystal is 0.6 mm.

Table 1
Crystal parameters, data-collection and processing statistics.

Values in parentheses are for the highest resolution shell. 2.5 m*M* UO_2Ac_2 was required for high-resolution diffraction.

Crystal	Native	UAc
X-ray source	Rigaku RU-200	APS SERCAT 22-ID
Wavelength (Å)	1.5418	0.997
Detector	R-AXIS IV	MAR 300
Space group	$P2_12_12$	$P2_12_12$
Unit-cell parameters (Å)		
a	170.83	165.65
b	238.04	236.19
c	76.372	75.87
Resolution range (Å)	50–6.0 (6.21–6.0)	50–2.92 (2.96–2.92)
No. of observations	65977	137413
Unique reflections	6634	64207
Mosaicity (°)	1.1	0.67
Completeness (%)	79.2 (64.0)	96.9 (69.7)
Average $\langle I/\sigma(I)\rangle$	11.4 (3.2)	22.8 (2.35)
$R_{\rm merge}$ (%)	0.063 (0.224)	0.151 (0.26)
No. of crystals	1	3

We have put much effort into extending the resolution limits of the VSV N protein–RNA crystals. As discussed previously, alternative crystallization conditions have successfully pushed the resolution from crystals exhibiting no diffraction to 10 Å and finally to 6 Å. Two potential factors that have limited further increases in diffraction are the presence of the RNA and the large size (∼500 kDa; Green *et al.*, 2000) of the assembled macromolecular complex. We have attempted to overcome each of these issues. The RNA in this complex is heterogeneous in sequence and was bound during protein expression. Two avenues have been pursued to eliminate this problem. One has been to replace the RNA with a homogeneous population of RNA. This was attempted at the point of protein expression by transcribing VSV-specific RNAs concomitant with N and P protein expression. Our preliminary results suggested that in the bacterial system the N protein did not preferentially select the specific RNAs and rather bound to the heterogeneous population of RNAs in the cell (unpublished data). However, this is not to suggest a lack of specificity for RNA binding, but rather a limitation of our

bacterial system. The other approach was to eliminate the RNA. At basic pH, naked RNA will undergo base-catalyzed hydrolysis during which the 2′-OH on the nucleotides is deprotonated and the adjacent 3′-phosphate undergoes nucleophilic attack by this deprotonated 2′-O. This results in cleavage of the RNA. In order to induce a similar cleavage of the RNA bound to the N protein, the N protein–RNA oligomer was incubated in phosphate buffer at pH 11 for several days. Interestingly, complexes treated in this manner still contained fully intact RNA, which suggested that the N protein bound and protected the 2′-OH of the RNA (Green *et al.*, 2000). Lastly, we have made attempts to proteolytically cleave the N protein. The rabies virus N protein was shown to be cleaved specifically by trypsin, resulting in the loss of a 17 kDa fragment from its amino-terminus (Iseni *et al.*, 1998; Kouznetzoff *et al.*, 1998). The VSV N protein can also be cleaved at a single site by trypsin (Arg127). However, efforts to remove this fragment from the larger oligomer once cleavage was complete were unsuccessful. Thus, the assembled N protein–RNA oligomer has proved to be quite stable.

In efforts to screen for heavy-atom derivatives, we unexpectedly obtained an interesting result with crystals soaked in the presence of uranyl acetate (UAc). Crystals soaked stepwise in increasing amounts of UAc (final concentration of 2.5 m*M*) showed a large increase in diffraction quality and resolution. UAc-soaked crystals have diffracted to beyond 2.8 Å resolution, with routine diffraction between 3.5 and 3.0 Å. An example of the difference in diffraction for native and UAc-soaked crystals is shown in Fig. 2. This UAc-induced higher resolution diffraction was anisotropic in the direction of *a**, with a drop-off observed beyond 4.5 Å. The unit-cell parameters and data statistics for UAc-soaked crystals are shown in Table 1. Crystals suffered from radiation damage during the course of data collection. As a result, partial data sets from three crystals were merged in order to obtain the complete high-resolution data set presented in Table 1. The $R_{\rm merge}$ values for each individual data set, 4.3, 5.4 and 10.4, were considerably lower than the combined value of 15.1%. Merging of the two crystals with the lower individual $R_{\rm merge}$ values resulted in a more reasonable combined $R_{\rm merge}$ of 9.0% but an incomplete data set. Thus, the marginal data set from the third crystal was used to obtain more complete data. The increase of the combined $R_{\rm merge}$ value is potentially a consequence of slight nonisomorphism. Analysis using the methods of Matthews (1968) revealed that there is half a decamer per asymmetric unit, with a $V_{\rm M}$ of 2.93 Å^3 Da^{-1}, corresponding to a solvent content of 57%, all of which is consistent with the native crystals. Implications of crystal packing on the anisotropic diffraction will be discussed later.

Self-rotation functions were calculated to search for non-crystallographic symmetry elements. The N protein–RNA complex is likely to have a tenfold rotation axis through the

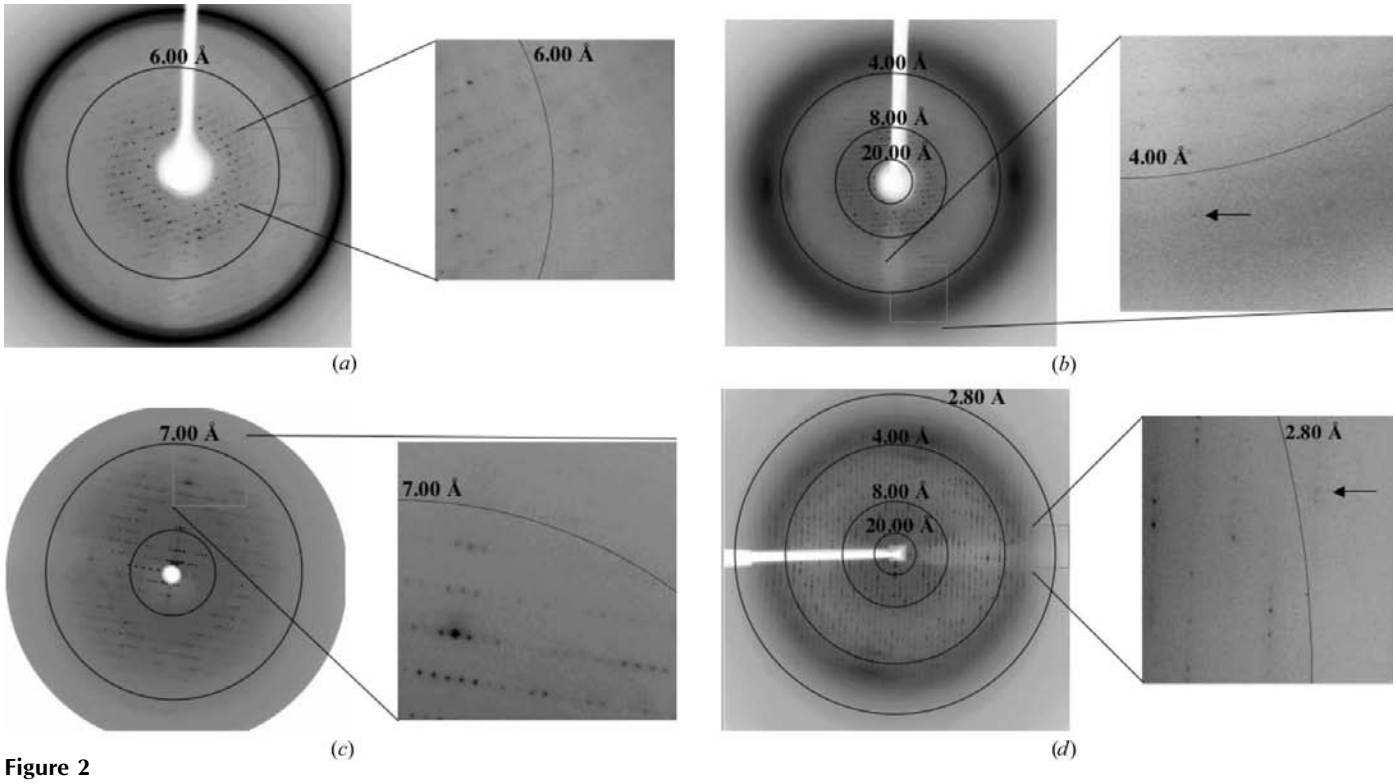

Figure 2
Differences in diffraction for native VSV N protein–RNA *versus* UAc-soaked crystals. The images in (*a*) and (*b*) were collected with home source equipment. Images (*c*) and (*d*) were collected at the synchrotron sources BioCars and SER-CAT, respectively. Native crystals (*a* and *c*) typically diffract to 7.5 Å, with the outlier in (*a*) diffracting to approximately 6 Å. Crystals soaked stepwise in UAc to a final concentration of 2.5 m*M* show a large increase in diffraction quality and resolution (*b* and *d*). High-resolution reflections to 3.73 and 2.74 Å resolution are noted with the aid of an arrow in (*b*) and (*d*), respectively. All images were collected at cryo-temperatures. Resolution rings for (*a*) 6.0, (*b*) 20.0, 8.0 and 4.0, (*c*) 20.0 and 7.0, (*d*) 40.0, 20.0, 8.0, 4.0 and 2.8 Å.

center of the disc (Chen *et al.*, 2004; Green *et al.*, 2000). The presence of a tenfold rotational axis and its orientation are given by a single peak on the stereographic plot for the $\kappa = 36^\circ$ section at $(\varphi, \psi) = (90, 90^\circ)$ (Fig. 3*a*). This suggests that the disc is oriented with the rotational axis parallel or coincident with the crystallographic *c* axis and is supported by the presence of a half-decamer in the asymmetric unit derived from the Matthews number. Concurrent with this is the presence of 20 peaks on the stereographic plot for $\kappa = 180^\circ$ (Fig. 3*b*). The 20 peaks are generated by the orientation of the tenfold in relation to the two orthogonal twofold screw axes. Although the oligomeric state was known prior to crystallization and EM had shown that the oligomer had the appearance of a disc suggesting a rotational symmetry (Green *et al.*, 2000), it was not known with absolute certainty whether the symmetry was a tenfold rotational symmetry or potentially five-two non-crystallographic symmetry. The tenfold rotational symmetry confirmed here was the same as the tenfold rotational symmetry identified recently from the negative-stain EM image reconstruction of the VSV N protein and RNA oligomer (Chen *et al.*, 2004).

3.1. Packing of the oligomer in the crystal

We have previously reported the dimensions of the N protein–RNA disc as determined by negative-stain EM (Chen *et al.*, 2004). The diameter and thickness of the disc were determined to be 16 and 8 nm, respectively. The tenfold rotation axis is through the center of the disc and thus perpendicular to the direction of the diameter of the disc (discussed earlier). Therefore, the disc sits with its thickness parallel to, if not coincident with, the crystallographic *c* axis and perpendicular to both the *a* and *b* axes. The thickness of the disc is consistent with the length of the *c* axis (75.71 Å). The difference in lengths between the thickness of the disc and the *c* axis suggests that discs from adjacent unit cells must intercalate slightly. From considerations of the diameter of the disc and the symmetry operators for the space group $P2_12_12$, the N protein must sit directly on the crystallographic twofold axis. This results in one half of the disc being crystallographically related to the other half. Interestingly, since the two halves of the disc are crystallographically related, any translation from the position on the *c* axis (a twofold) would disrupt the tenfold non-crystallographic symmetry of the disc. However, the position of the disc along the *c* axis cannot be deduced with the current analysis. Packing within the unit cell is illustrated in Fig. 4. The packing scheme in the crystal lattice places discs from adjacent unit cells in the direction of the *c* axis, sitting perfectly one upon another and creating extended 'tubes' of the N protein. By symmetry operation, a second tube is centered at $(x, y) = (0.5, 0.5)$ and in an inverted orientation relative to the orientation of the disc at (0, 0). This packing suggests some intercalation of the barrel-shaped disc in the directions perpendicular to the *c* axis. The diameter of 160 Å determined by electron microscopy (Chen *et al.*, 2004) also suggests that there might be a lack of contact or a minimal amount of contact along the direction of the *a* axis (which is 165.65 Å). This could lead to flexibility in that direction. This disorder could explain why the crystals diffract anisotropically.

3.2. Resolution improvement of N protein–RNA crystals

Modification of the protein as well as the crystallization conditions was performed in the hope of achieving higher

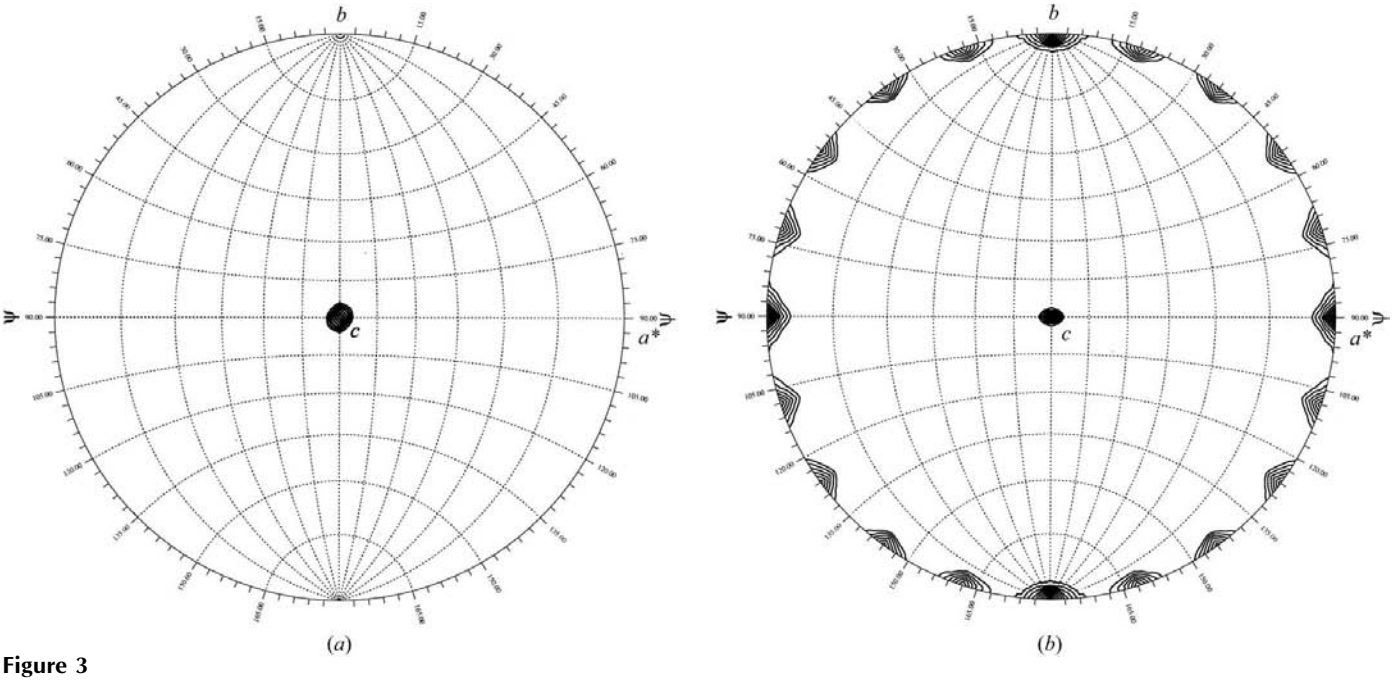

Figure 3
Self-rotation function calculated with the VSV N protein–RNA crystals. Self-rotation searches with (*a*) $\kappa = 36^\circ$ and (*b*) $\kappa = 180^\circ$ were used to identify tenfold and twofold rotation angles, respectively. Contours for (*a*) start at 6 standard deviations (sd) with intervals of 2 sd and for (*b*) start at 2 sd with intervals of 1 sd. Analysis and plots produced with *GLRF* (Tong & Rossmann, 1997).

resolution diffraction from the N protein–RNA crystals. The method employed that yielded the desired results was the introduction of uranyl ions into previously grown crystals. Stepwise soaking of crystals in UAc resulted in a dramatic difference in diffraction (Fig. 2). The concentration of the heavy atom was critical to the diffraction limits, as crystals soaked in concentrations below 2.5 m*M* uranyl acetate had diffraction limits that were equivalent to those of native crystals, while increasing beyond this concentration showed no additional improvement.

A search through the PDB and literature yielded examples of other proteins that have been dependent on uranyl ions for successful crystal growth or increases in diffraction. In the case of OppA from *Salmonella typhimurium*, initial crystal growth resulted in thin fragile crystals that were difficult to reproduce (Tolley *et al.*, 1988). Addition of uranium to the crystallization condition was necessary to stabilize the crystal growth, which resulted in thicker crystals that diffracted to 2.1 Å (Glover *et al.*, 1995; Tame *et al.*, 1994). The lattice stabilization was the result of a uranyl ion which bound to an Asp and a Glu residue between crystallographically related molecules. The YloQ protein from *Bacillus subtilis* is another example of uranyl addition which increased diffraction, in this instance from 2.50 to 1.6 Å (Levdikov *et al.*, 2004). Here, the uranyl ions stabilize the N-terminus of the protein. The asparaginyl-tRNA synthetase from *Thermus thermophilus* is another case (Berthet-Colominas *et al.*, 1998). The result of uranyl binding here is the stabilization of the lattice of the crystal. This is achieved by binding of uranyl between molecules lying in between crystal contact positions. It is reasonable to guess that in the crystals of the N protein, the protein, RNA or both are stabilized or charges are neutralized by the additional of uranium. In the cases mentioned above, the UO_2^{2+} ion predominantly binds to the negatively charged residues glutamic and aspartic acid. The N protein has 17 and 35 of these residues, respectively. This accounts for 4.03 and 8.29% of the protein, respectively. This is a significant increase in aspartic acid over the average of 5.5% (Klapper, 1977). This could suggest that proteins with several negatively charged residues could potentially benefit from uranyl binding.

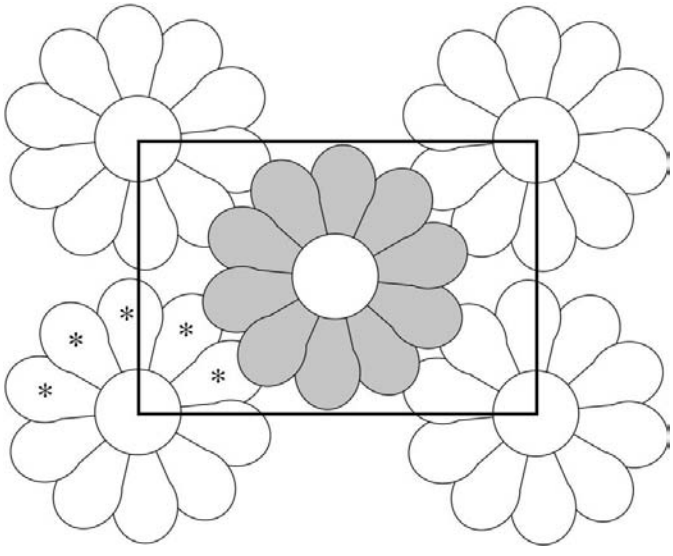

Figure 4
Schematic plots of a possible packing arrangement of the N protein decamer in the $P2_12_12$ unit cell. The crystallographic twofold (the *c* axis) is perpendicular to the plane of the page. The asymmetric unit is filled with a half-decamer of the N protein. Each monomer is denoted with an asterisk. The second half of the disc is generated by the twofold crystallographic symmetry. The placement of the disc along the *c* axis is unknown and is arbitrary. In the cartoon, the shaded disc is flipped 180° with respect to the *y* axis, giving non-shaded and shaded discs an up or down orientation, respectively.

The improvement in the X-ray diffraction quality by soaking crystals in uranyl acetate was not only a solution for the N protein–RNA complex, but also may be a general method for obtaining crystals that produce X-ray diffraction data at high resolution. Diffraction quality is a major obstacle in protein structure determination by X-ray crystallography, as illustrated by the fact that only about 20% of all protein crystals produced by the structural genomics effort diffracted X-rays to better than 3 Å (Liu *et al.*, 2005). A number of methods that change the surface charged residues have been shown to be effective in improving crystal diffraction quality. For instance, mutations have been introduced to change surface Lys or Arg residues to Ala residues of the protein RhoGDI (Longenecker *et al.*, 2001). Change of as little as a single surface Lys residue to Ala residue yielded protein crystals that were suitable for structure determination. Likewise, a single Lys to Ile mutation produced diffraction-quality crystals of cyclophilin D (Schlatter *et al.*, 2005). Another method is to methylate surface Lys residues (Rayment *et al.*, 1993). A protein from *Pyrococcus furiosus*, Pfu-392566, yielded crystals that diffracted X-rays to 1.2 Å resolution only after methylation of surface Lys residues (Liu *et al.*, 2005). The improvement of crystal quality appears to be the result of reduction in surface entropy of the protein or stabilization of crystal contacts. Soaking in uranyl acetate may be a rescuing method to improve crystal quality after growing native crystals as opposed to protein modification prior to crystallization. Neutralization of the negatively charged surface residues by counterions may be a cost-effective method to rescue some of the 80% of protein crystals that fail to produce high-resolution X-ray data, especially those that may have a large number of negatively charged surface residues.

To date, there are no homologous structures available for attempts to phase the current data by the molecular-replacement method. In addition, the location of uranium sites in Patterson maps calculated from the difference between data from native and UAc-soaked crystals has proved to be difficult owing to a lack of isomorphism between crystals. Non-isomorphism was not surprising since there is such a large increase in the diffraction limits following derivatization of the crystals with UAc. The uranium could structurally stabilize either the protein or protein–protein contacts within the crystals. Thus, the stabilization is likely to render the crystals non-isomorphous. Our current focus is to exploit the anomalous signal of uranium for phase information. Preparation for data collection is currently under way.

We thank the staff of the South-East Regional Collaborative Access Team (SER-CAT) at the Advanced Photon Source for their assistance in data collection. Use of the Advanced Photon Source was supported by the US Department of Energy, Office of Science, Office of Basic Energy Sciences under Contract No. W-31-109-Eng-38. This work is supported in part by a grant to ML (NIH, AI050066).

References

Berthet-Colominas, C., Seignovert, L., Härtlein, M., Grotli, M., Cusack, S. & Leberman, R. (1998). *EMBO J.* **17**, 2947–2960.
Blumberg, B. M. & Kolakofsky, D. (1983). *J. Gen. Virol.* **64**, 1839–1847.
Chen, Z., Green, T. J., Luo, M. & Li, H. (2004). *Structure*, **12**, 227–235.
Emerson, S. U. & Wagner, R. R. (1972). *J. Virol.* **10**, 297–309.
Emerson, S. U. & Yu, Y. (1975). *J. Virol.* **15**, 1348–1356.
French, S. & Wilson, K. (1978). *Acta Cryst.* A**34**, 517–525.
Glover, I. D., Denny, R. C., Nguti, N. D., McSweeney, S. M., Kinder, S. H., Thompson, A. W., Dodson, E. J., Wilkinson, A. J. & Tame, J. H. R. (1995). *Acta Cryst.* D**51**, 39–47.
Green, T. J., MacPherson, S., Qiu, S., Lebowitz, J., Wertz, G. W. & Luo, M. (2000). *J. Virol.* **74**, 9515–9524.
Huang, A. S. & Wagner, R. R. (1966). *J. Mol. Biol.* **22**, 381–384.
Iseni, F., Barge, A., Baudin, F., Blondel, D. & Ruigrok, R. W. (1998). *J. Gen. Virol.* **79**, 2909–2919.
Jancarik, J. & Kim, S.-H. (1991). *J. Appl. Cryst.* **24**, 409–411.
Keene, J. D., Thornton, B. J. & Emerson, S. U. (1981). *Proc. Natl Acad. Sci. USA*, **78**, 6191–6195.
Klapper, M. H. (1977). *Biochem. Biophys. Res. Commun.* **78**, 1018–1024.
Kouznetzoff, A., Buckle, M. & Tordo, N. (1998). *J. Gen. Virol.* **79**, 1005–1013.
Leslie, A. G. W. (1992). *Jnt CCP4/ESF–EACBM Newsl. Protein Crystallogr.* **26**.
Levdikov, V. M., Blagova, E. V., Brannigan, J. A., Cladiere, L., Antson, A. A., Isupov, M. N., Seror, S. J. & Wilkinson, A. J. (2004). *J. Mol. Biol.* **340**, 767–782.
Liu, Z. J. *et al.* (2005). *J. Struct. Funct. Genomics*, **6**, 121–127.
Longenecker, K. L., Garrard, S. M., Shefield, P. J. & Derewenda, Z. S. (2001). *Acta Cryst.* D**57**, 679–688.
McPherson, A. (1982). *Preparation and Analysis of Protein Crystals.* New York: John Wiley.
Matthews, B. W. (1968). *J. Mol. Biol.* **33**, 491–497.
Otwinowski, Z. & Minor, W. (1997). *Methods Enzymol.* **276**, 307–326.
Qanungo, K. R., Shaji, D., Mathur, M. & Banerjee, A. K. (2004). *Proc. Natl Acad. Sci. USA*, **101**, 5952–5957.
Rayment, I., Rypniewski, W. R., Schmidt-Base, K., Smith, R., Tomchick, D. R., Benning, M. W., Winkelmann, D. A., Wesenberg, G. & Holden, H. M. (1993). *Science*, **261**, 50–58.
Schlatter, D., Thoma, R., Kung, E., Stihle, M., Muller, F., Borroni, E., Cesura, A. & Hennig, M. (2005). *Acta Cryst.* D**61**, 513–519.
Schoehn, G., Iseni, F., Mavrakis, M., Blondel, D. & Ruigrok, R. W. (2001). *J. Virol.* **75**, 490–498.
Tame, J. R. H., Murshudov, G. N., Dodson, E. J., Neil, T. K., Dodson, G. G., Higgins, C. F. & Wilkinson, A. J. (1994). *Science*, **264**, 1578–1581.
Thomas, D., Newcomb, W. W., Brown, J. C., Wall, J. S., Hainfeld, J. F., Trus, B. L. & Steven, A. C. (1985). *J. Virol.* **54**, 598–607.
Tolley, S. P., Derewenda, Z., Hyde, S. C., Higgins, C. F. & Wilkinson, A. J. (1988). *J. Mol. Biol.* **204**, 493–494.
Tong, L. & Rossmann, M. G. (1997). *Methods Enzymol.* **276**, 594–611.